Supplemental Materials

Molecular Biology of the Cell

Hertzler *et al*.

Supplementary Figure 1. Localization patterns of cid, Ndc80, and overexpressed Nuf2.
(A) GFP-cid, eGFP-Spc25, and UAS-eGFP-Nuf2 flies were crossed to a line containing 221-Gal4 and UAS-mCD8-mCherry. Left column, cell shape; middle column, fluorescent protein of interest; right column, merged images.

Supplementary Figure 2. Localization of low-expressing tagged kinetochore constructs.
(A) eGFP-Ndc80, Mis12-GFP, and gTub37c RNAi flies (a "no-GFP" control) were crossed to a line containing 221-Gal4 and UAS-iBlueberry as a cell shape marker. Left column, cell shape; middle column, fluorescent protein of interest; right column, merged images.

Supplementary Figure 3. Dendrite regeneration of class IV ddaC neurons is slightly reduced by kinetochore protein knockdowns.
(A) Diagram of class IV ddaC neuron regeneration. All dendrites are severed proximal to the cell body (red arrows); by 24 hours, a robust new dendrite arbor has formed, and is quantified by measuring the maximum diameter of the new arbor (red line). Example images of regeneration for control, Ndc80, and AurB RNAi's are shown. Average regeneration diameter is plotted for control and kinetochore RNAi in **(B)**. Numbers in columns are numbers of neurons analyzed. ***, $p<.001$; **, $p<.01$, with a Kruskal-Wallis one-way anova, each experimental genotype compared to the control with Dunn's multiple comparisons test. Error bars are standard deviation.

Supplementary Figure 4. Class IV ddaC neurons have increased microtubule dynamics with kinetochore protein knockdowns.
(A) Overview of class IV ddaC neuron showing regions analyzed for microtubule dynamics. Each segment has the number of EB1 puncta counted and divided by the segment length and are averaged together per neuron. **(B)** Example kymographs of one dendrite segment from control (left) and Ndc80 RNAi knockdown (right). **(C)** Average microtubule dynamics are plotted for the RNAi lines tested. ***, $p<.001$ with a Kruskal-Wallis one-way anova, each experimental genotype compared to the control with Dunn's multiple comparisons test. Error bars show standard deviation.

Supplementary Figure 5. Kinetochore protein knockdown may affect microtubule turnover in dendrites but not axons.
(A) tdEOS-αTub, a photoconvertible tubulin monomer, is turned from green to red by 405nm light. The loss of red converted tdEOS from a region is an indicator of microtubule turnover. Example images display the fluorescence intensity of converted regions immediately after conversion and one hour later for control and Ndc80 RNAi. The average intensity of red fluorescence remaining in the converted region in either axons or dendrites at 1 and 1.5 hours is quantified as a percentage remaining from the initial conversion and plotted in **(B)**. While close, no significance arises between any genotypes and control with a Kruskal-Wallis one-way anova. Numbers in columns are number of neurons analyzed. Note that every cell had regions of both dendrites and axons converted sequentially in separate acquisitions. Axons and dendrites were analyzed separately. Error bars show standard deviation.

Supplementary Figure 6. Knockdown of kinetochore proteins does not change many metrics of microtubule polymerization.

(A and C) Kymographs displaying how polymerization speed and run length are measured (green lines and red lines with brackets, respectively). Speed is calculated as distance (microns, x axis measurement) divided by time (seconds, y axis measurement) for each polymerization event in a kymograph. **(B)** Average comet speed is quantified for control and kinetochore RNAi genotypes. Numbers in columns are number of comets quantified, generated from 3-7 videos per genotype. **(D)** Average run length is plotted for control and kinetochore RNAi genotypes. Only comets whose start and end point were both present in a kymograph were counted. Numbers in columns are total number of comets quantified, from 7-12 kymographs generated from each genotype. No significance arises between control and any other group using a Kruskal-Wallis one-way anova. **(E and F)** Polarity (direction of polymerization) is quantified for each comet seen in both axons and dendrites. Data is plotted as a percentage of comets traveling away from the cell body (axons) or toward from the cell body (dendrites). Numbers in columns represent total number of comets present in all videos taken per genotype. Note that comet speed, run length, and dendrite polarity in (B), (D), and (F) respectively are taken from the same videos from which microtubule dynamics were quantified and shown in Figure 4B. Error bars show standard deviation.

Supplementary Figure 7. Positive control for GNE-3511 DLK inhibitor demonstrates effectiveness in reducing microtubule dynamics caused by cell stress.
(A) Kymographs of videos taken of neurons expressing RNAi for unc-104 with either DMSO or GNE-3511 applied. Microtubule dynamics are quantified in an identical manner to Figure 4 and are plotted in **(B).** ***, $p<.001$ in an unpaired t test with Welch's correction between unc-104 with and without GNE-3511. Note that control DMSO and GNE-3511 data is the same as depicted in Figure 5B. Numbers in columns are number of neurons analyzed. Error bars show standard deviation.

Supplementary Figure 8. Core nucleation protein γTub23C levels are not changed by knockdown of kinetochore proteins.
(A) Control, Ndc80, and borr RNAi's were crossed to a line containing 221-Gal4, UAS-iBlueberry, and γTub23C-sfGFP (expressed under its endogenous promoter). Example images of control and borr RNAi are shown. **(B)** Quantification of green channel fluorescence in the soma of ddaE neurons per genotype. Neither Ndc80 nor borr RNAi genotypes are significantly different from control with a Kruskal-Wallis one-way anova. Numbers in columns are numbers of neurons analyzed. Error bars show standard deviation.

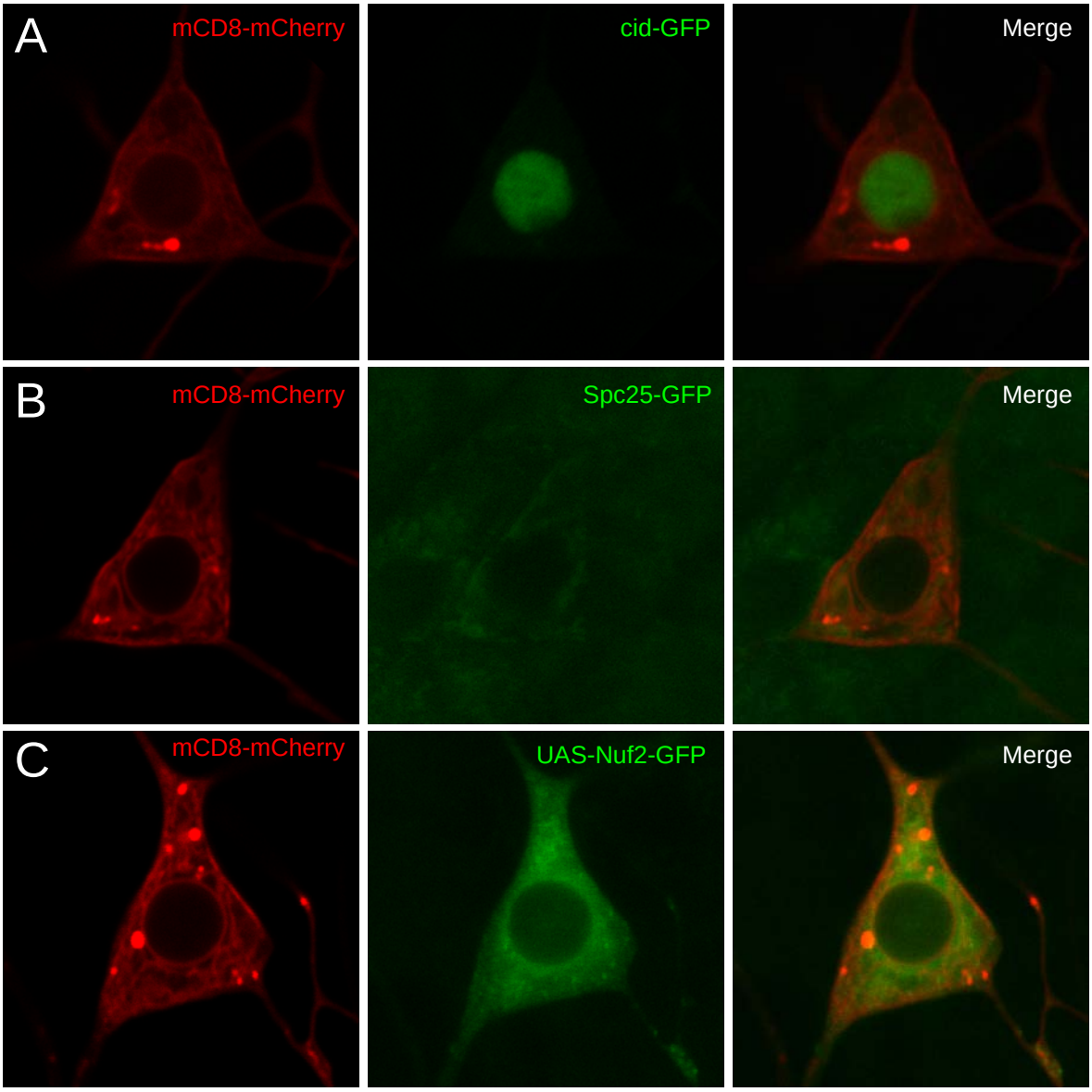
A
mCD8-mCherry
cid-GFP
Merge
B
mCD8-mCherry
Spc25-GFP
Merge
C
mCD8-mCherry
UAS-Nuf2-GFP
Merge

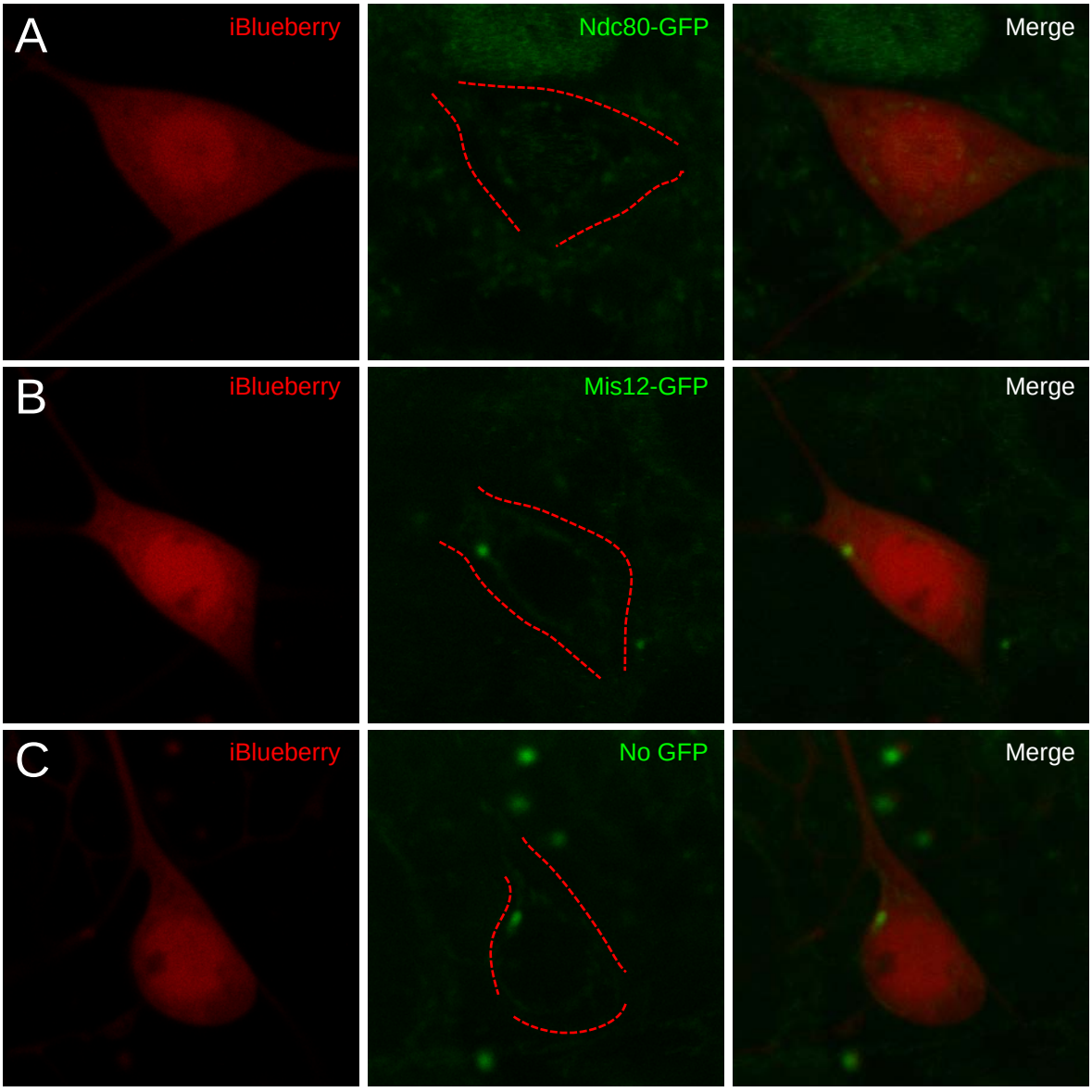
A
iBlueberry
Ndc80-GFP
Merge
B
iBlueberry
Mis12-GFP
Merge
C
iBlueberry
No GFP
Merge

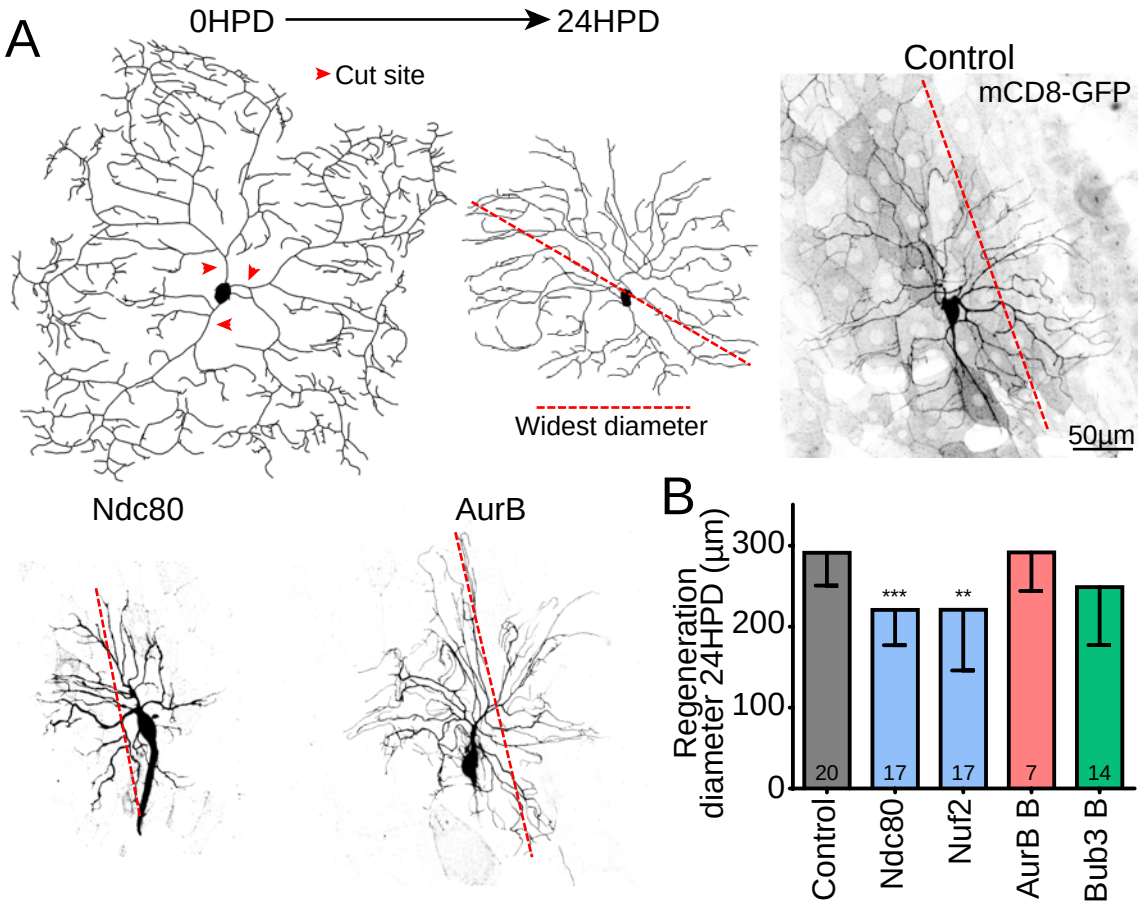
A
0HPD
24HPD
Cut site
Widest diameter
Control
mCD8-GFP
50µm
Ndc80
AurB
B
Regeneration diameter 24HPD (µm)
300
200
100
0
***
**
20
17
17
7
14
Control
Ndc80
Nuf2
AurB B
Bub3 B

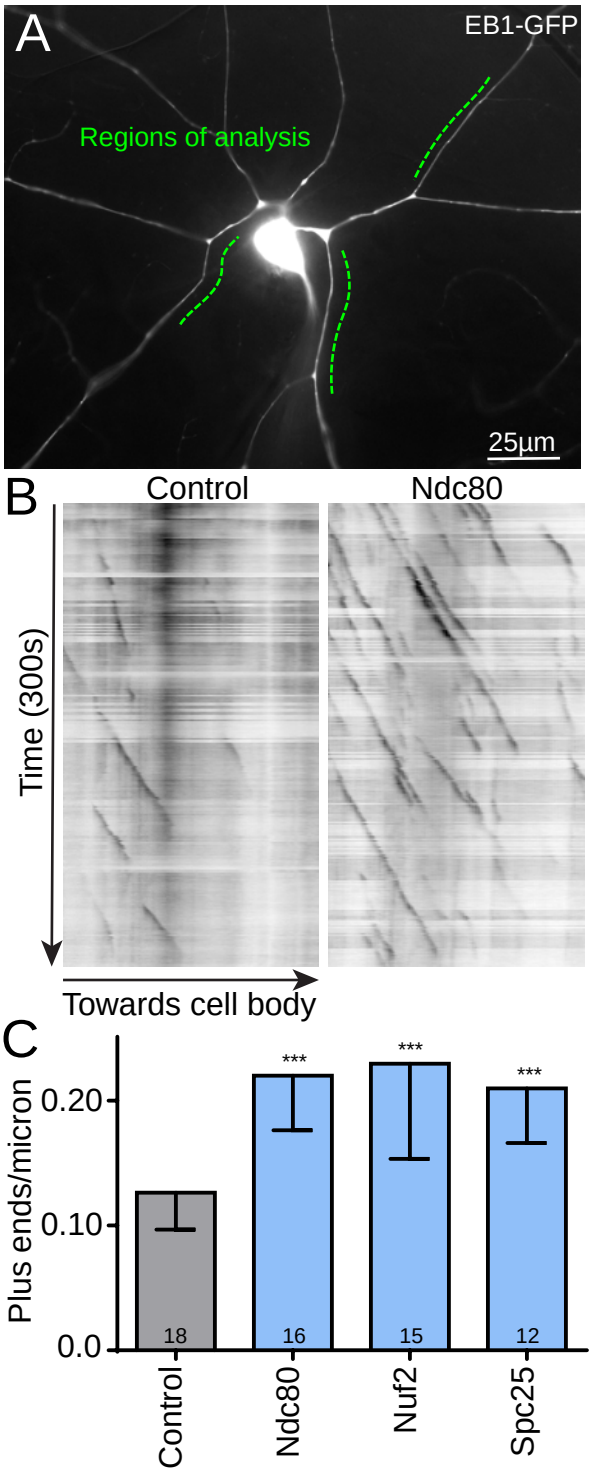
A
EB1-GFP
Regions of analysis
25µm
B
Control
Ndc80
Time (300s)
Towards cell body
C
Plus ends/micron
0.20
0.10
0.0
***
***
***
18
16
15
12
Control
Ndc80
Nuf2
Spc25

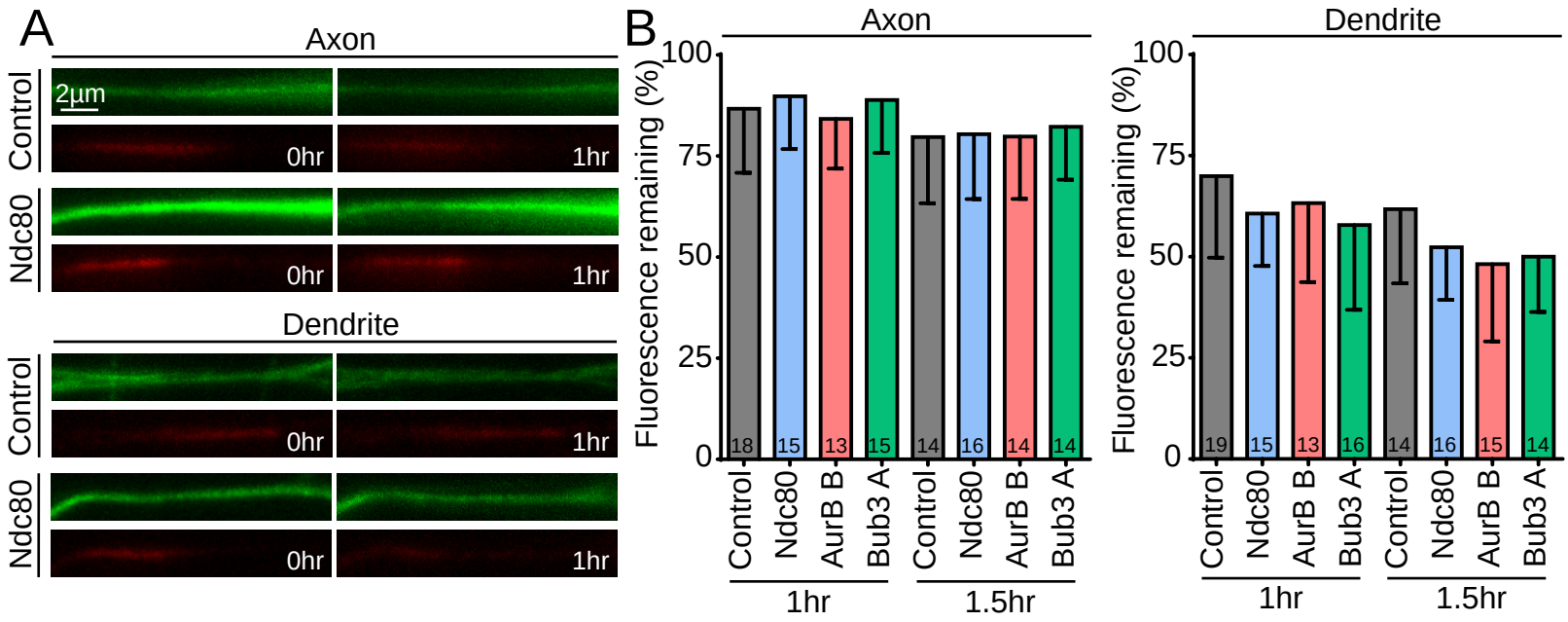
A
Axon
Control
2µm
0hr
1hr
Ndc80
0hr
1hr
Dendrite
Control
0hr
1hr
Ndc80
0hr
1hr
B
Axon
Fluorescence remaining (%)
100
75
50
25
0
18
15
13
15
14
16
14
14
Control
Ndc80
AurB B
Bub3 A
Control
Ndc80
AurB B
Bub3 A
1hr
1.5hr
Dendrite
Fluorescence remaining (%)
100
75
50
25
0
19
15
13
16
14
16
15
14
Control
Ndc80
AurB B
Bub3 A
Control
Ndc80
AurB B
Bub3 A
1hr
1.5hr

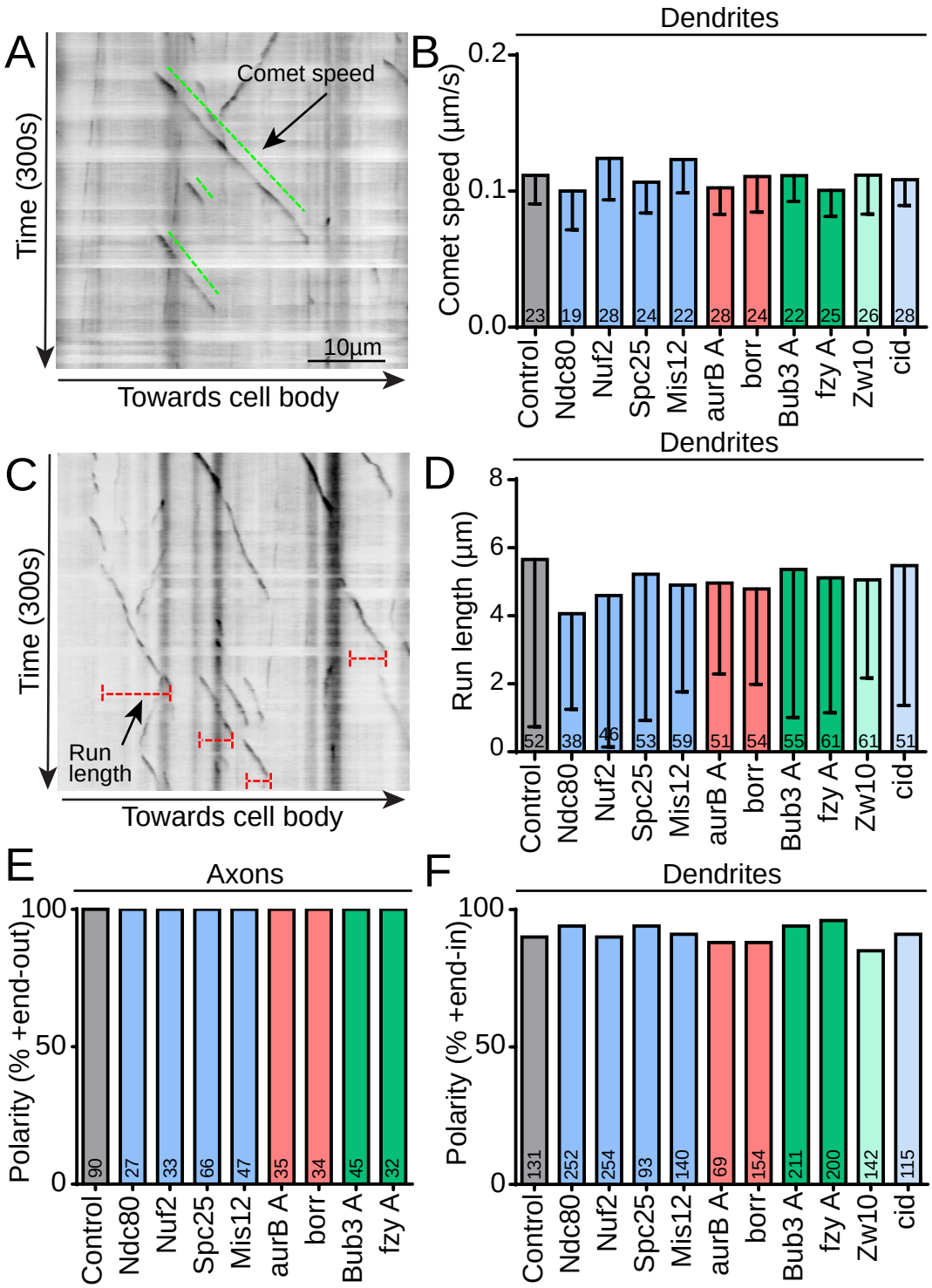
A
Time (300s)
Comet speed
10µm
Towards cell body
B
Dendrites
Comet speed (µm/s)
0.2
0.1
0.0
23
19
28
24
22
28
24
22
25
26
28
Control
Ndc80
Nuf2
Spc25
Mis12
aurB A
borr
Bub3 A
fzy A
Zw10
cid
C
Time (300s)
Run length
Towards cell body
D
Dendrites
Run length (µm)
8
6
4
2
0
52
38
46
53
59
51
54
55
61
61
51
Control
Ndc80
Nuf2
Spc25
Mis12
aurB A
borr
Bub3 A
fzy A
Zw10
cid
E
Axons
Polarity (% +end-out)
100
50
0
90
27
33
66
47
35
34
45
32
Control
Ndc80
Nuf2
Spc25
Mis12
aurB A
borr
Bub3 A
fzy A
F
Dendrites
Polarity (% +end-in)
100
50
0
131
252
254
93
140
69
154
211
200
142
115
Control
Ndc80
Nuf2
Spc25
Mis12
aurB A
borr
Bub3 A
fzy A
Zw10
cid

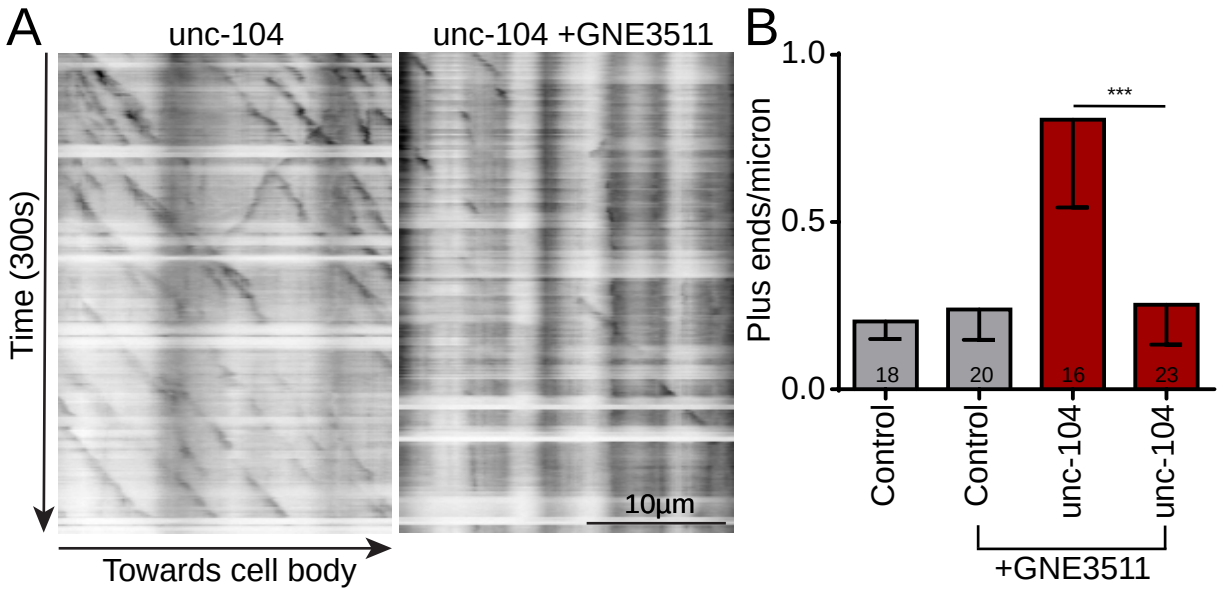
A
unc-104
unc-104 +GNE3511
Time (300s)
Towards cell body
10µm
B
Plus ends/micron
1.0
0.5
0.0
***
18
20
16
23
Control
Control
unc-104
unc-104
+GNE3511

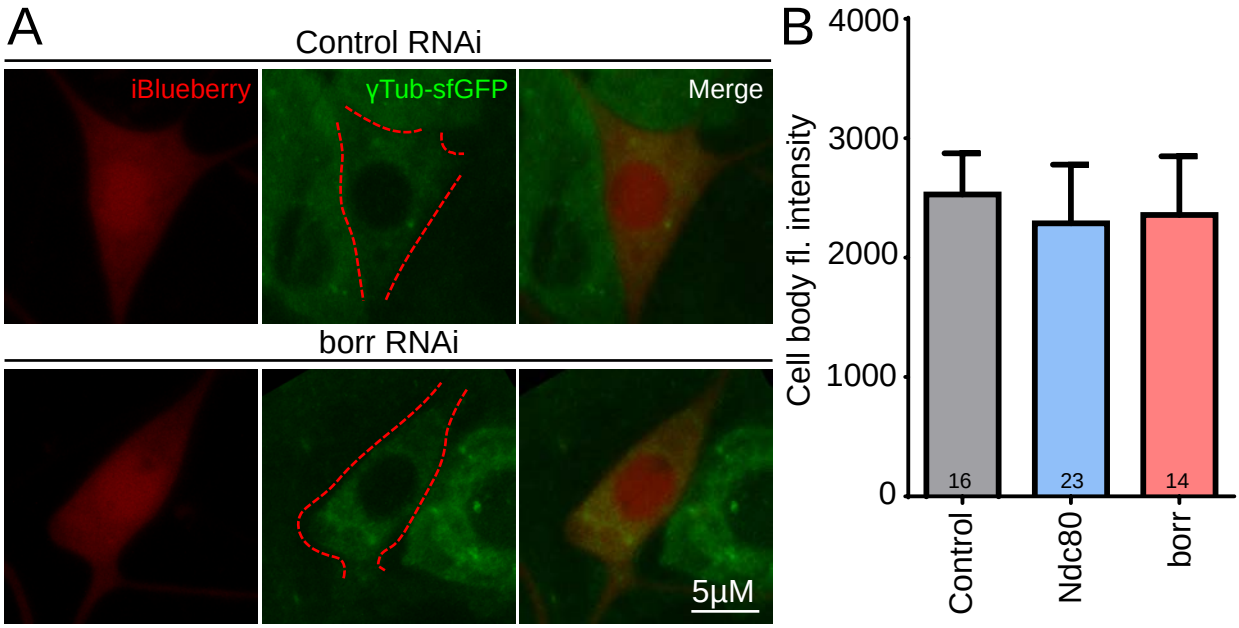
A
Control RNAi
iBlueberry
γTub-sfGFP
Merge
borr RNAi
5μM
B
Cell body fl. intensity
4000
3000
2000
1000
0
16
23
14
Control
Ndc80
borr

Table 1. RNASeq reads from uninjured ddaC neurons and neurons 6h after dendrite removal.
Four pools of RNA from 10 neurons were generated for control and injured neurons (Den6) and short read single-end reads were generated using Illumina HiSeq. Reads were assigned to Drosophila genes, and raw counts for the four injured replicates are shown in columns E to H and for the four control replicates are shown in columns I to L. The average injured reads were compared to uninjured and the list is ranked with most upregulated at the top (this is represented as Log 2-fold change in column C). Note that this data is noisy because of the low amount of starting material.

Table 2. List of Drosophila lines and other reagents.
A complete list of reagents used in this study is included.

Table 3. Raw data for all quantitation.
The Table contains the numerical data used to generate all the graphs.